INTERNATIONAL JOURNAL FOR NUMERICAL METHODS IN FLUIDS
Int. J. Numer. Meth. Fluids **28**: 1217–1239 (1998)

APPLICATION OF THE FULL APPROXIMATION STORAGE METHOD TO THE NUMERICAL SIMULATION OF TWO-DIMENSIONAL STEADY INCOMPRESSIBLE VISCOUS MULTIPHASE FLOWS

C.P. THOMPSON* AND P. LEZEAU

Applied Mathematics and Computing Group, School of Mechanical Engineering, Cranfield University, UK

SUMMARY

In recent years multigrid algorithms have been applied to increasingly difficult systems of partial differential equations and major improvements in both speed of convergence and robustness have been achieved. Problems involving several interacting fluids are of great interest in many industrial applications, especially in the process and petro-chemical sectors. However, the multifluid version of the Navier–Stokes equations is extremely complex and represents a challenge to advanced numerical algorithms. In this paper, we describe an extension of the full approximation storage (FAS) multigrid algorithm to the multifluid equations. A number of special issues had to be addressed. The first was the development of a customised, non-linear, coupled relaxation scheme for the smoothing step. Automatic differentiation was used to facilitate the coding of a robust, globally convergent quasi-Newton method. It was also necessary to use special inter-grid transfer operators to maintain the realisability of the solution. Algorithmic details are given and solutions for a series of test problems are compared with those from a widely validated, commercial code. The new approach has proved to be robust; it achieves convergence without resorting to specialised initialisation methods. Moreover, even though the rate of convergence is complex, the method has achieved very good reduction factors: typically five orders of magnitude in 50 cycles. © 1998 John Wiley & Sons, Ltd.

KEY WORDS: multiphase; multifluid; multigrid; FAS; local coupled solver

1. INTRODUCTION

For the simulation of single-phase viscous flow, the combination of a multigrid procedure and local quasi-Newton iterative schemes leads to very efficient and robust solvers for the Navier–Stokes equations (see e.g. References [1,2]). The extension of this methodology to multiphase flows is *a priori* promising: in multiphase flows, variables are very tightly and locally coupled together. In such cases, a local quasi-Newton method may converge significantly faster than algorithms which rely on global, rather than local, linearisations, and therefore constitute a good smoother on which a fast multigrid method can be built.

Our starting point is a parallel, adaptive, multigrid, local quasi-Newton coupled solver for two-dimensional steady Navier–Stokes flows on staggered grids called pamg [3–5]. Its

* Correspondence to: Applied Mathematics and Computing Group, School of Mechanical Engineering, Cranfield University, Cranfield, Beds., MK43 OAL, UK. Tel: +44 1234 754634; Fax: +44 1234 750728; E-mail: chris.thompson@cranfield.ac.uk

CCC 0271–2091/98/181217–23$17.50

Received October 1997
Revised February 1998

extension to multiphase flows, pamg-multiphase, requires a careful treatment because the differential operators are far more complex. This is the main object of this paper.

Having defined the equations considered, their discretisation in a finite volume framework is discussed in section 2 using hybrid first–second-order schemes. In Section 3 the coupled solver which is at the heart of the algorithm is described. In Section 4 the embedding of this solver in a multigrid method is considered. Finally, in Sections 5 and 6, some results establishing the accuracy and efficiency of our implementation are presented. Our main goal is to illustrate the potential of our approach and investigate some of the outstanding issues for optimised performance.

2. MULTIPHASE MODEL AND DISCRETISED EQUATIONS

2.1. Basic equations

Multiphase flow is a very challenging problem from the standpoint of numerical simulation as well as physical modelling, particularly if transient phenomena are considered. Consequently it has attracted attention for a long time [6–10]. In this study, the multiphase flow model used is the well-known multifluid model [11] where the phases are assumed to be interpenetrating continua and macroscopic balance equations are derived by an averaging process. We consider here the flow of M incompressible viscous fluids. In principle, each phase could have its own pressure field but we apply a single pressure model instead and adopt the following governing equations:

- M continuity equations of the form

$$\nabla \cdot (r_\alpha \mathbf{u}_\alpha) = 0, \tag{1}$$

- M momentum equations of the form

$$\nabla \cdot (r_\alpha(\rho_\alpha \mathbf{u}_\alpha \otimes \mathbf{u}_\alpha - \mathbf{T}_\alpha)) = -r_\alpha \nabla p_\alpha + \sum_{\beta=1}^{M} c_{\alpha\beta}(\mathbf{u}_\beta - \mathbf{u}_\alpha), \tag{2}$$

- M constitutive relationships for the viscous stresses

$$\mathbf{T}_\alpha = \mu_\alpha(\nabla \mathbf{u}_\alpha + (\nabla \mathbf{u}_\alpha)^T), \tag{3}$$

- One closure relationship for the volume fractions

$$\sum_{\alpha=1}^{M} r_\alpha = 1, \tag{4}$$

$M-1$ closure relationships for the pressures

$$p_1 = p_2 = \cdots = p_{M-1}, \tag{5}$$

where the subscripts α and β are phase identifiers. This constitutes a system of $4M$ equations for $4M$ unknowns: r_α, u_α, v_α and p_α for each phase.

There is no transfer of mass between the phases but this could easily be done. Transfer of momentum is allowed and modelled by algebraic source terms. In this study a simple momentum transfer model is adopted, known as the mixture model. We take

$$c_{\alpha\beta} = \frac{C_D}{d_{\alpha\beta}} \rho_{\alpha\beta} r_\alpha r_\beta |\mathbf{u}_\beta - \mathbf{u}_\alpha|, \tag{6}$$

where the drag coefficient C_D and the interfacial length scale $d_{\alpha\beta}$ are known functions of the flow and $\rho_{\alpha\beta}$, the mixture specific mass, is defined as

$$\rho_{\alpha\beta} = r_\alpha \rho_\alpha + r_\beta \rho_\beta.$$

2.2. Discretisation methods and choices

The partial differential equations (1) and (2) are discretised on a staggered grid (see Figure 1) by a finite volume approach which ensures that numerical fluxes are exactly conserved at cells boundaries.

Consider first the continuity equations. Some care is needed to obtain stable finite volume approximations to the actual partial differential equations. The momentum equations are then considered and hybrid schemes are used in order to avoid instabilities associated with large cell Reynolds numbers on coarse grids [12]. This extends the methodology used in the single phase case. The details of the derivation of the discretised conservation equations can be found in Reference [13]. Its main stages and the results are given here. In order to simplify the notations, the phase identifiers are dropped everywhere in this section, except for the momentum inter-phase transfer terms.

2.3. Discretisation of the continuity equations

By integrating Equation (1) over a single cell, applying Green's theorem and dividing by the area $\Delta x \Delta y$ of the cell, the discrete continuity equations can be written

$$\frac{[ru]_{i+1/2,\,j} - [ru]_{i-1/2,\,j}}{\Delta x} + \frac{[rv]_{i,\,j+1/2} - [rv]_{i,\,j-1/2}}{\Delta y} = 0. \tag{7}$$

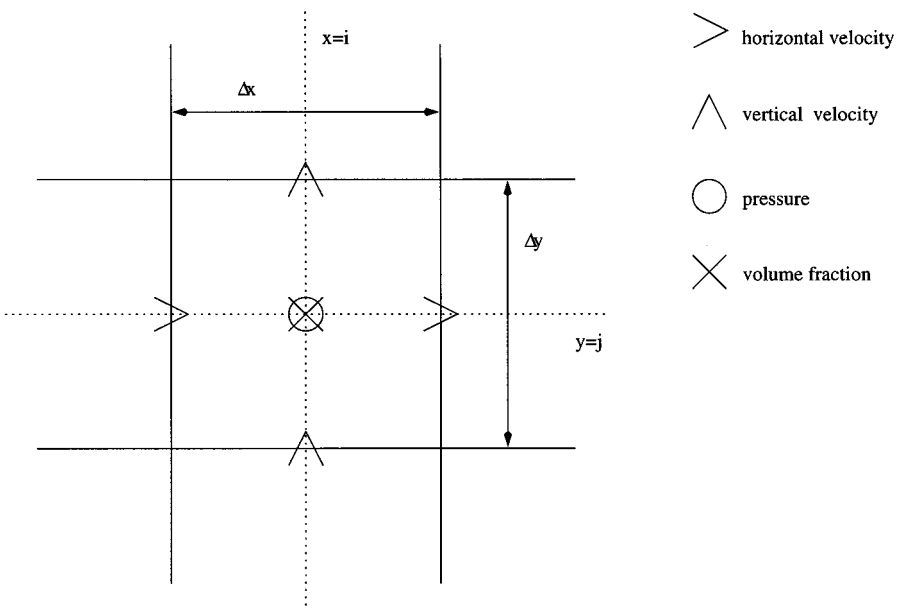

Figure 1. Arrangement of the staggered grid.

A staggered grid is used, therefore, all values of r referred must be interpolated. A first obvious choice is geometric interpolation, giving, e.g. $r_{i+1/2,j} \equiv \frac{1}{2}(r_{i+1,j} + r_{i,j})$ and $r_{i,j+1/2} \equiv \frac{1}{2}(r_{i,j+1} + r_{i,j})$. This is second-order-accurate. However, if Equation (7) is then rewritten as

$$\left(\frac{1}{2\Delta x}\, u_{i+1/2,\,j}\right) r_{i+1,\,j} - \left(\frac{1}{2\Delta x}\, u_{i-1/2,\,j}\right) r_{i-1,\,j} + \left(\frac{1}{2\Delta y}\, v_{i,\,j+1/2}\right) r_{i,\,j+1} - \left(\frac{1}{2\Delta y}\, v_{i,\,j-1/2}\right) r_{i,\,j-1}$$
$$+ \left[\frac{1}{2\Delta x}\,(u_{i+1/2,\,j} - u_{i-1/2,\,j}) + \frac{1}{2\Delta y}\,(v_{i,\,j+1/2} - v_{i,\,j-1/2})\right] r_{i,\,j} = 0,$$

the derivative of the (discrete) mass flux with respect to the volume fraction r_{ij} is

$$\frac{1}{2\Delta x}\,(u_{i+1/2,\,j} - u_{i-1/2,\,j}) + \frac{1}{2\Delta y}\,(v_{i,\,j+1/2} - v_{i,\,j-1/2}).$$

This expression may take small values, expressing the fact that the numerical coupling between the volume fraction and the continuity residual is weak. Since large corrections are then generated, geometric interpolation for the volume fractions in the continuity equations leads to instabilities which prevent convergence. In order to obtain a stable discretisation, a first-order-accurate upwind interpolation is used for the volume fraction; e.g.

$$r_{i+1/2,\,j} \equiv \frac{1}{2}\left[(1 - \mathrm{sgn}(u_{i+1/2,\,j}))\, r_{i+1,\,j} + (\mathrm{sgn}(u_{i+1/2,\,j}) + 1)\, r_{i,\,j}\right],$$

where sgn is the sign function: $\mathrm{sgn}(\alpha) = -1$ if $x < 0$ and $\mathrm{sgn}(x) = 1$ if $x \geq 0$.

2.4. Discretisation of the momentum equations

The discretisation of the momentum equations is straightforward and can be performed by integrating Equation (2) over a rectangular control volume of size $(\Delta x, \Delta y)$ centred around velocity locations, applying Green's theorem and dividing by $\Delta x\, \Delta y$. Hybrid differencing is introduced by selecting an upwind or a centred interpolation formula for the velocities according to the (discrete) ratio of convective and diffusive terms. The diffusive flux $\nabla \cdot (r\mathbf{T})$ involves extra terms compared with the single-phase equations:

$$\mu \nabla \cdot (r[\nabla \mathbf{u} + (\nabla \mathbf{u})^T]) = \mu \begin{pmatrix} 2(r u_x)_x + [r(u_y + v_x)]_y \\ [r(v_x + u_y)]_x + 2(r v_y)_y \end{pmatrix}. \tag{8}$$

When only one phase is present ($r = 1$), this expression simplifies to the usual Newtonian stress tensor:

$$\mu \begin{pmatrix} u_{xx} + u_{yy} \\ v_{xx} + v_{yy} \end{pmatrix},$$

by application of the continuity equation (1). For multiphase flows, such a simplification is not possible and the resulting cross derivative terms can affect the convergence speed of the solver. This is discussed further in Section 6.4.

The discretised momentum equations for phase α are

$$A^u_C u_{i+1/2,\,j} = A^u_E u_{i+3/2,\,j} + A^u_N u_{i+1/2,\,j+1} + A^u_W u_{i-1/2,\,j} + A^u_S u_{i+1/2,\,j-1} + (V_N - V_S)$$
$$- \frac{r_E}{\rho \Delta x}\,(p_{i+1,\,j} - p_{i,\,j}) + \frac{[Q^u_\alpha]_{i+1/2,\,j}}{\rho}, \tag{9}$$

$$A^v_C v_{i,\,j+1/2} = A^v_E v_{i+1,\,j+1/2} + A^v_N v_{i,\,j+3/2} + A^v_W v_{i-1,\,j+1/2} + A^v_S v_{i,\,j-1/2} + (U_E - U_W) - \frac{r_N}{\rho \Delta y}(p_{i,\,j+1} - p_{i,\,j}) + \frac{[Q^v_\alpha]_{i,\,j+1/2}}{\rho}, \tag{10}$$

where Q^u_α and Q^v_α are the discretisations of the inter-phase momentum transfer terms which are algebraic; e.g.

$$[Q^u_1]_{i+1/2,\,j} = -[Q^u_2]_{i+1/2,\,j} = C_D(\rho_1[r_1]_E + \rho_2[r_2]_E)\frac{[r_1]_E[r_2]_E}{d_{12}}\,|[u_2]_{i+1/2,\,j} - [u_1]_{i+1/2,\,j}|([u_2]_{i+1/2,\,j} - [u_1]_{i+1/2,\,j}).$$

V_N, V_S, U_E and U_W are terms encapsulating the multiphase diffusive cross-derivative terms. In sharp contrast with the continuity equations, the interpolation procedures for the volume fractions have proved to be non-critical. In particular, we have been able to use second-order-accurate geometric interpolation formulae. Briefly, the various coefficients appearing in Equation (9) are defined as follows. The diagonal term is given by

$$A^u_C = A^u_E + A^u_N + A^u_W + A^u_S, \tag{11}$$

where the transport terms are of the form

$$A^u_E = \max(2D^u_e, |C^u_e|) - C^u_e, \tag{12}$$

and similarly for A^u_W, A^u_N and A^u_S. Note that there is no factor 2 in the diffusive contributions for A^u_N and A^u_S (see Equation (8)). The convective terms follow the form

$$C^u_e = \frac{1}{4\Delta x}(u_{i+1/2,\,j} + u_{i+3/2,\,j})r^u_e,$$

while the diffusive terms are given by expressions of the type

$$D^u_e = \frac{\nu}{\Delta x^2} r^u_e.$$

Additionally, the cross derivative diffusive terms are discretised as follows:

$$V_N = \frac{1}{\Delta x\ \Delta y}\nu r^u_n(v_{i+1,\,j+1/2} - v_{i,\,j+1/2}), \qquad V_S = \frac{1}{\Delta x\ \Delta y}\nu r^u_s(v_{i+1,\,j-1/2} - v_{i,\,j-1/2}).$$

It remains to define the volume fractions:

$$r_E = \frac{1}{2}(r_{i+1,\,j} + r_{i,\,j}), \qquad r^u_e = r_{i+1,\,j}, \qquad r^u_w = r_{i,\,j},$$

$$r^u_n = \frac{1}{4}(r_{i,\,j} + r_{i+1,\,j} + r_{i+1,\,j+1} + r_{i,\,j+1}), \qquad r^u_s = \frac{1}{4}(r_{i,\,j} + r_{i+1,\,j} + r_{i+1,\,j-1} + r_{i,\,j-1}).$$

The terms involved in the discrete vertical momentum equation are very similar. This discretisation is first-order-accurate due to the use of upwind interpolation in the continuity equations. The momentum equations are second-order-accurate for sufficiently small grid sizes because hybrid differencing is used.

A range of boundary conditions are possible. At walls, we have non-slip conditions for the velocities and $\partial_n r = 0$. At outlets, fully developed flow is assumed.

3. SOLUTION METHOD

3.1. Design

Given discretised equations defined at appropriate nodes on a grid, a large system of non-linear algebraic equations must be solved. This is achieved by an iterative procedure known as the symmetrical coupled Gauss–Seidel method (SCGS) introduced by Vanka [1]: for each iteration, we consider every computational cell in the domain ordered in lexicographic order, write a local system of equations which is therefore much smaller and correct the unknowns with a single Newton step. This process is repeated until the residual, measured by an appropriate vector norm, is small enough.

This approach (i) takes into account the strong local coupling between dependent variables and (ii) provides a local linearisation with good smoothing properties on which an efficient multigrid method can be added. See References [1,3] for its application to single-phase problems.

3.2. The local Newton method

If we consider a single computational cell (i, j), 12 equations can be written for the 12 unknowns defined on that cell. For each phase, a continuity equation, two horizontal momentum equations centred around the points $(i-1/2, j)$ and $(i+1/2, j)$ respectively and two horizontal momentum equations centred around the points $(i, j-1/2)$ and $(i, j+1/2)$ respectively, can be written. The problem is closed by

$$[p_1]_{i,j} - [p_2]_{i,j} = 0,$$

and

$$[r_1]_{i,j} + [r_2]_{i,j} = 1,$$

to obtain a non-linear system of algebraic equations:

$$\mathbf{f}(\mathbf{\Phi}) = 0, \tag{13}$$

where

$$\mathbf{\Phi} = ([u_1]_{i-1/2,j}\ [u_1]_{i+1/2,j}\ [v_1]_{i,j-1/2}\ [v_1]_{i,j+1/2}\ [p_1]_{i,j}\ [u_2]_{i-1/2,j}\ [u_2]_{i+1/2,j}\ [v_2]_{i,j-1/2}\ [v_2]_{i,j+1/2}\ [p_2]_{i,j}\ [r_1]_{i,j}\ [r_2]_{i,j})^T,$$

If J denotes the Jacobian of $\mathbf{f}$ on the cell (i, j) with respect to $\mathbf{\Phi}$, and $\mathbf{\Phi}^{(n)}$ is an approximation of the solution $\mathbf{\Phi}$ of Equation (13), then the Newton correction $\Delta\mathbf{\Phi}$ is defined by

$$J\Delta\mathbf{\Phi} = -\mathbf{f}(\mathbf{\Phi}^{(n)}). \tag{14}$$

After inversion of this system, the approximation of the solution can be updated: $\mathbf{\Phi}^{(n+1)} = \mathbf{\Phi}^{(n)} + \Delta\mathbf{\Phi}$.

3.2.1. Expressions for the Jacobian. In such a Newton method, the key problem is to compute J. This may be cumbersome as the number of variable increases. Also, the presence of boundaries may complicate the derivation of correct expressions.

In some cases, the expressions for J can be approximated: in the single-phase pamg code for instance, J is obtained after approximating $\mathbf{f}(\mathbf{\Phi})$ by $A(\mathbf{\Phi})\mathbf{\Phi}$ and neglecting the non-diagonal velocity entries. Experimental evidence seems to suggest that in the case of multiphase flow, the expressions for the Jacobian need to be much more accurate than in the single-phase case, due

to the increased degree of non-linearity. In particular, a straightforward extension of the expressions derived in Reference [4] has proved insufficient to ensure the convergence of the method.

In the present study, *automatic differentiation* was used to obtain expressions for the Jacobian. The particular software used, the AD01 package of the Harwell Subroutine Library [14], is not a pre-processor but a collection of routines which compute the derivatives of an expression at run-time by relying on the operator overloading capabilities of fortran90. This has important advantages for code development:

- it automatically ensures that the Jacobian and the residual in Equation (14) are consistent with each other;
- different discretisation options can be tested easily with minimal code writing.

When a good discretisation has been obtained, the Jacobian can be computed in an optimised way.

3.2.2. Globally convergent Newton methods. It is well known that Newton's method is not globally convergent: if the initial guess is not close enough to the actual solution, the method may fail because it takes corrective steps which are too large. This is particularly true if the condition number of J is large.

For single-phase flow computations, the failure of the local Newton method to converge usually indicates an error in the computer code. For multiphase computations, in contrast, we have consistently observed that the basic Newton method fails to converge. An obvious hypothesis is that the system solved is much more non-linear than in the single-phase case.

In order to make the Newton method convergent, we have supplemented it with line searching [15]. Given the correction step $\Delta\mathbf{\Phi}$ defined by Equation (14), the new approximation of the solution is defined by

$$\mathbf{\Phi}^{(n+1)} = \mathbf{\Phi}^{(n)} + \lambda\Delta\mathbf{\Phi}. \tag{15}$$

The scaling factor λ is chosen so that the correction reduces the Euclidean norm of $\mathbf{f}$:

$$\left\|\mathbf{\Phi}^{(n+1)}\right\|_2 < \left\|\mathbf{\Phi}^{(n)}\right\|_2. \tag{16}$$

It is always possible to find λ for which Equation (16) is satisfied because the direction of the Newton correction is a descent direction for the Euclidean norm. The only exception is the case where the approximation is a local minimum, but in practice, this does not cause any problems.

3.2.3. Relaxation. Although line searching can be thought of as an intelligent underrelaxation procedure, it is not sufficient alone to ensure convergence on fine grids. This was remedied by the application of additional underrelaxation with factors ranging from 0.6 to 0.8. This is far higher than the value used with conventional methods.

4. MULTIGRID COMPUTATIONS

Multigrid methods are fast solvers, originally developed for elliptic partial differential equations [16–20] which have been successfully applied to other types of partial differential equations as well as non-differential problems [21].

By combining a local quasi-Newton solver and a multigrid method, we aim at designing an algorithm which will be fast and robust. The two procedures are complementary in the sense that they deal effectively with high and low frequencies in the error respectively.

In this study, the *full approximation storage* (FAS) variant of the multigrid method has been implemented. It has been specifically developed for systems of non-linear equations, as opposed to the *correction storage* (CS) scheme which is restricted to linear equations. An overview of the solution algorithm together with the grid transfer operators used for multiphase flows are given in this section. Details of the implementation for single-phase flows and multiphase flows can be found in References [4] and [13] respectively.

4.1. FAS solution algorithm

We define a sequence of successively finer *uniform* grids $k = 1, \kappa$ such that

$$\Delta x_k = \Delta y_k = \frac{1}{2}\Delta x_{k-1} = \frac{1}{2}\Delta y_{k-1}, \quad k = 2, \kappa.$$

We seek to solve, on the finest grid $k = \kappa$, the non-linear system of algebraic equations:

$$\mathscr{L}_\kappa(w_\kappa) = f_\kappa.$$

In FAS, as with CS, given an approximation $\tilde{w}_\kappa^{(n)}$ of the solution w_κ, we seek to compute a correction $\Delta\tilde{w}_\kappa$ to give the next approximation of the solution: $\tilde{w}_\kappa^{(n+1)} = \tilde{w}_\kappa^{(n)} + \Delta\tilde{w}_\kappa$. This correction is computed on the next coarser grid $k = \kappa - 1$ so that the low frequencies of the fine grid error can be more effectively damped. This coarse grid correction is then interpolated back to the fine grid using a prolongation operator $I_{\kappa-1}^{\kappa}$: $\Delta\tilde{w}_\kappa = I_{\kappa-1}^{\kappa}(\Delta\tilde{w}_{\kappa-1})$. The difference between the FAS and CS schemes arises from the definition of the coarse grid problem. In the CS scheme, the coarse grid correction is obtained by solving a residual equation. Consequently, only the fine grid residuals need to be interpolated to the coarse grid. In FAS, the error equation has to be modified due to the non-linearity of the problem. It is necessary to restrict to the coarse grid both the residuals and the approximation of the fine grid solution, using two restriction operators, $I_\kappa^{\kappa-1}$ and $\hat{I}_\kappa^{\kappa-1}$ respectively.

The following problem is therefore posed on the coarse grid:

$$\mathscr{L}_{\kappa-1}(\tilde{w}_{\kappa-1}) = f_{\kappa-1},$$

with

$$f_{\kappa-1} \equiv I_\kappa^{\kappa-1}(f_\kappa - \mathscr{L}_\kappa(\tilde{w}_\kappa)) + \mathscr{L}_{\kappa-1}(\hat{I}_\kappa^{\kappa-1}\tilde{w}^k).$$

The coarse grid correction is then defined as

$$\Delta\tilde{w}_{\kappa-1} \equiv \tilde{w}_{\kappa-1} - \hat{I}_\kappa^{\kappa-1}(\tilde{w}_\kappa).$$

4.2. Grid transfer operators for multiphase flows

Given a multigrid single-phase code such as pamg, the adaptation for multiphase flows requires chiefly (i) a restriction operator for the volume fractions and (ii) a prolongation operator for the volume fraction corrections. Velocities and pressures are handled in the same way as in single-phase flows in both the restrictions and prolongation steps. Setting $if = 2ic$ and $jf = 2jc$, we have

- restriction of the velocities; e.g.

$$u_{ic+1/2,\,jc}^{(c)} = \frac{1}{2}\left(u_{if+1/2,\,jf-1}^{(f)} + u_{if+1/2,\,jf}^{(f)}\right), \tag{17}$$

- restriction of the pressures:

$$p^{(c)}_{ic,\,jc} = \frac{1}{4}\,(p^{(f)}_{if-1,\,jf-1} + p^{(f)}_{if-1,\,jf} + p^{(f)}_{if-1,\,jf} + p^{(f)}_{if,\,jf}), \tag{18}$$

- prolongation of the velocities corrections; for the horizontal component, this takes the form

$$\Delta u^{(f)}_{if+1/2,\,jf} = \Delta u^{(c)}_{ic+1/2,\,jc} + \frac{1}{8}\,\Delta u^{(c)}_{ic+1/2,\,jc+1} - \frac{1}{8}\,\Delta u^{(c)}_{ic+1/2,\,jc-1}. \tag{19}$$

  The correction for the vertical velocities are defined in a similar way. These operators are not the 'standard' operators for the prolongation of a edge-defined quantity. They are actually a modification of these operators so that for single-phase flows, mass fluxes are conserved by the prolongation. This property, which the usual prolongation operators do not share, is crucial for the successful implementation of adaptive gridding [3]. For multiphase flows, the operator (19) needs to be modified further to ensure the conservation of mass fluxes.
- prolongation of the pressures corrections: we can choose either first-order interpolation

$$\Delta p^{(f)}_{if,\,jf} = \Delta p^{(f)}_{if,\,jf-1} = \Delta p^{(f)}_{if-1,\,jf} = \Delta p^{(f)}_{if-1,\,jf-1} = \Delta p^{(c)}_{ic,\,jc}, \tag{20}$$

  or, alternatively, second-order formulae of the type

$$\Delta p^{(f)}_{if,\,jf} = \frac{1}{16}\,(9\Delta p^{(c)}_{ic,\,jc} + 3\Delta p^{(c)}_{ic+1,\,jc} + 3\Delta p^{(c)}_{ic,\,jc+1} + \Delta p^{(c)}_{ic+1,\,jc+1}). \tag{21}$$

The transfer of residuals to coarser grids can be done using simple operators. Firstly, the residuals for the closure relationships (4) and (5) are always zero on all grids, provided they are satisfied by the initial guess, and therefore do not need to be restricted.

The residuals of the momentum equations are defined on cell edges. Therefore, the same operators are used as for the velocities. The horizontal momentum residuals are restricted using Equation (17), while the vertical momentum equations are restricted using a similar expression. The continuity residuals are cell-centred and accordingly, Equation (18) is used for their restriction to the coarse grid.

It remains to define transfer operators for the volume fractions. Since they are cell-centred quantities, the same operators as for the pressure are used, i.e. Equations (18) and (20) are used for the restriction and the prolongation respectively. If the second-order-accurate prolongation procedure is chosen instead, it is necessary to pay attention to the treatment of the boundary values. In order to keep the operator as simple as possible, we have opted for first-order prolongation. Although conventional multigrid wisdom indicates that higher order of accuracy is advisable for the grid transfer operators, in the present form of the algorithm, interpolation errors do not appear to be predominant [13].

4.3. Prolongation and physically admissible solutions

When fine grid volume fractions are restricted to the next coarser grid, it is impossible to generate non-physical values on the coarse grid, provided that all volume fractions take physically acceptable values on the fine grid. This is due to the existence of a maximum principle which insures that the interpolated values are bounded by the interpolants. By contrast, in the prolongation stage, it is possible to correct the fine grid volume fractions in such a way that they become non-physical. Obviously, this is more likely when residuals are still high or when the solution field for the volume fractions locally approaches one or zero.

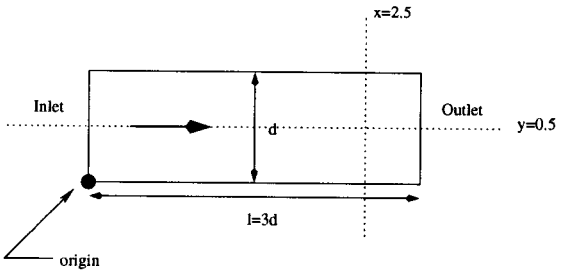

Figure 2. Geometry of the two-phase channel flow problem.

When non-physical values are generated, the multigrid algorithm, not surprisingly, quickly diverges. The solution is to test the fine grid values after correction and reset them to physical values if necessary:

$$\begin{array}{l} \text{if} \quad r_{ij}^{(f)} > 1, \quad \text{set} \quad r_{ij}^{(f)} = 1 - \epsilon \\ \text{if} \quad r_{ij}^{(f)} < 0, \quad \text{set} \quad r_{ij}^{(f)} = \epsilon \end{array}, \tag{22}$$

where ϵ is a small number (typically 10^{-6}), added so that correction systems are not made singular by the presence of an exactly zero volume fraction. Alternatively, corrections may be discarded if they lead to non-physical values for the volume fractions:

$$\begin{array}{l} \text{if} \quad r_{ij,\text{old}}^{(f)} + \Delta r_{ij} > 1, \quad \text{set} \quad r_{ij,\text{new}}^{(f)} = r_{ij,\text{old}}^{(f)} \\ \text{if} \quad r_{ij,\text{old}}^{(f)} + \Delta r_{ij} < 0, \quad \text{set} \quad r_{ij,\text{new}}^{(f)} = r_{ij,\text{old}}^{(f)} \end{array}. \tag{23}$$

The results presented here have been obtained using the second procedure.

4.4. Cycling strategies

It remains to specify the cycling strategy to completely define the multigrid solver. 'V' cycles are not applicable, due to the high degree of non-linearity. Instead, we have chosen 'F' cycles which are often as robust as the 'W' cycles but less costly. Computations always start on the coarsest grid as in the full multigrid procedure. Two SCGS sweeps are performed after a prolongation and a further two before a restriction. The same SCGS smoother [4] is used on the coarsest grid, rather than a direct solver.

5. ACCURACY OF THE SOLVER

This section aims at validating our implementation and assessing the accuracy of our two-phase computations. Full details as well as other test cases can be found in Reference [13].

5.1. Problem 1: Two-phase channel flow

5.1.1. Problem definition. Firstly, we consider a two-phase flow in a channel. This is a very simple geometry. Nevertheless, phase separation renders the flow much more complicated than in the single-phase case. The computational domain (see Figure 2) is a simple rectangle with $0 < x < 3$, $0 < y < 1$. The coarsest grid defined contains 48 cells, and its resolution is $\Delta x_1 = \Delta y_1 = 0.25$. The fluids are defined by the following physical properties:

Reynolds number	Viscosity	Density
$Re_1 = 100$	$\mu_1 = 0.01$	$\rho_2 = 1.0$
$Re_2 = 100$	$\mu_2 = 0.005$	$\rho_2 = 0.5$

Here, the Reynolds number has been defined as a simple extension of the usual single-phase definition:

$$Re_\alpha = \frac{\rho_\alpha u_\alpha d}{\mu_\alpha}.$$

The characteristic length d is the channel width at the inlet. Inter-phase momentum transfers are not allowed for this case.

5.1.2. Main features of the solution. Since both phases share the same pressure field, the phase with less inertia is accelerated relative to the other (Figure 3(a,b)). As a result, there is significant flow separation as shown by the volume fraction field (Figure 3(c)). Along the main direction of the flow as well as across the channel width, it can clearly be seen that each phase has a very distinct velocity field (Figure 3(a,c)).

The result of the simulations also indicates that the flow evolves toward a layered pattern with the more viscous phase concentrated toward the sides of the channel (Figure 3(c)). This is likely to correspond to a minimal energy configuration.

5.1.3. Comparisons with CFX 4.1 solutions. The solutions given by pamg-multiphase have been compared with those provided by the well-validated CFX 4.1 code which uses the IPSA algorithm [22,23] to solve the same multifluid equations. Figure 4 shows that good agreement is obtained, although the solution algorithms are significantly different. For instance, CFX 4.1 uses non-staggered grids and Rhie-Chow interpolation to side-step the odd–even decoupling of the pressure.

5.1.4. Grid independence of the solutions. Studies of the grid independence of the solution have been carried out (see Figure 5). They support the conclusion that provided the finer grid is fine enough, the results provided by pamg-multiphase have a significant degree of grid independence. There is one exception: the volume fractions. Their evolution across the pipe is strongly dependent on the grid size (see Figure 5(b)). Figure 5(c) shows that the CFX 4.1 solutions share this feature to some extent, even though they are based on a different formulation. Hence, the fact that very fine grids are necessary to accurately resolve the volume fraction is likely to be a fundamental property of the equations as opposed to a characteristic of our discretisation.

5.2. Problem 2: Two-phase flow through a T-junction with two inlets

5.2.1. Problem description. In this second multiphase test problem, a two-phase flow through a T-junction with two inlets is considered. The aim is to demonstrate the correctness of the code for relatively complex flow patterns due to phase separation and mixing.

The two inlets case is simpler than the two outlets configuration because the extent of recirculation zones is minimised. In the context of multiphase flows, the presence of recirculation zones raises the issue of the well-posedness of the steady problem. If more than one phase is recirculating at one point, then the mass fractions of the recirculating phases are arbitrary and several solutions are possible.

The geometry of the problem is shown in Figure 6.

The operating fluids have the following physical properties (the Reynolds number is based on the channel width):

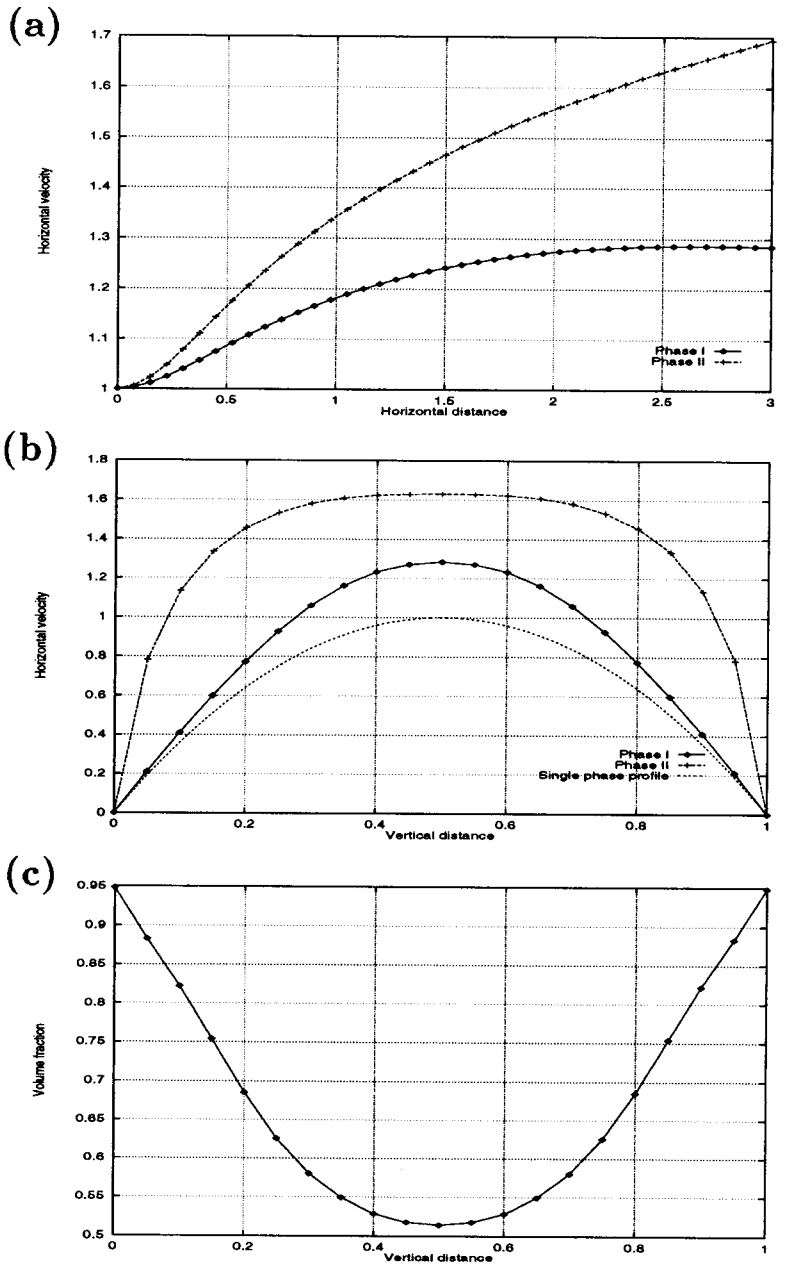

Figure 3. Two-phase channel flow—pamg-multiphase results—(a) horizontal velocity profiles along the line $y = 0.5$; (b) horizontal velocity profiles along the line $x = 2.5$; (c) volume fraction profile for phase 1 along the line $x = 2.5$.

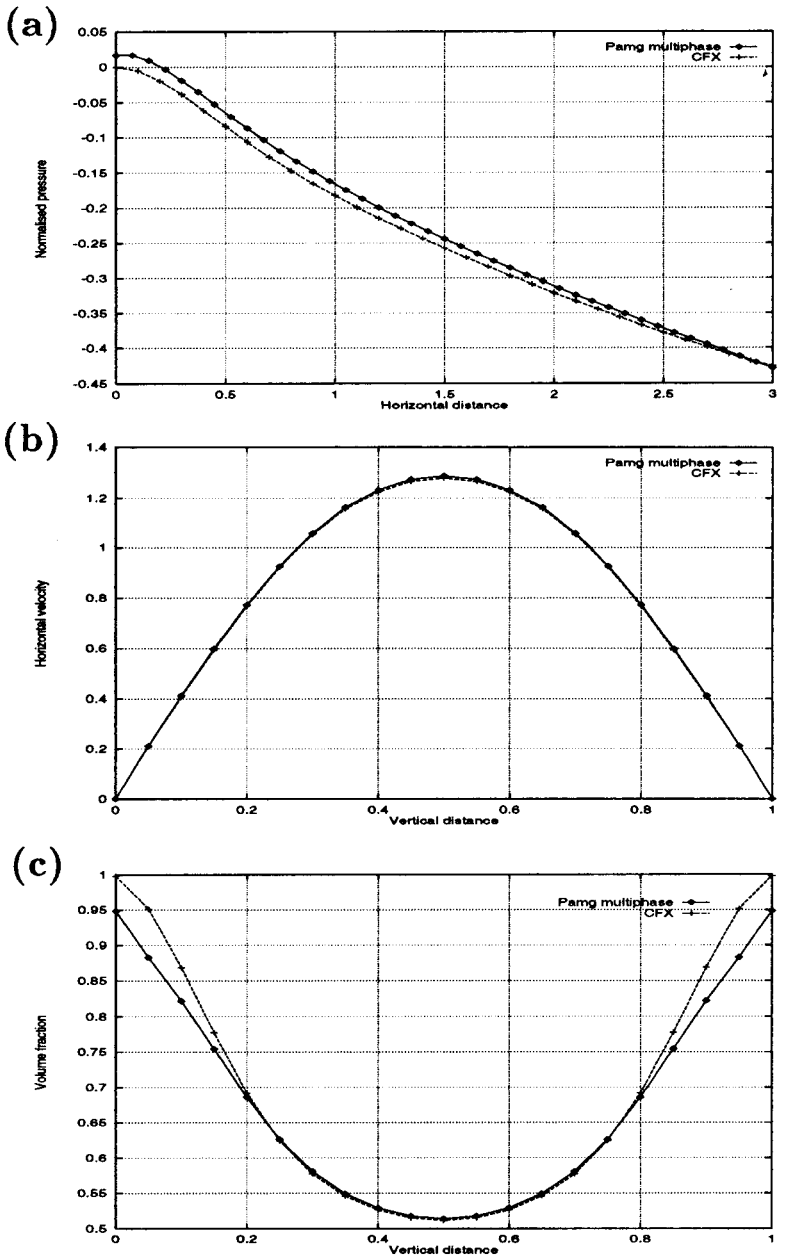

Figure 4. Two-phase channel flow—comparison of pamg-multiphase and CFX 4.1 results—(a) Pressure profiles along the line $y = 0.5$ (phase 1) after normalisation; (b) horizontal velocity profiles along the line $x = 2.5$ (phase 1); (c) volume fraction profiles along the line $x = 2.5$ (phase 1).

Reynolds number	Viscosity	Density
$Re_1 = 100$	$\mu_1 = 0.01$	$\rho_1 = 1.0$
$Re_2 = 75$	$\mu_2 = 0.0066$	$\rho_2 = 0.5$

For this test case, we allow inter-phase momentum transfers and use the mixture model given by Equation 6. For the sake of simplicity, the drag coefficient and the inter-facial length are constants rather than dependent on the state of the flow. The values are

$$C_D = 1, \qquad d_{\alpha\beta} = 0.1.$$

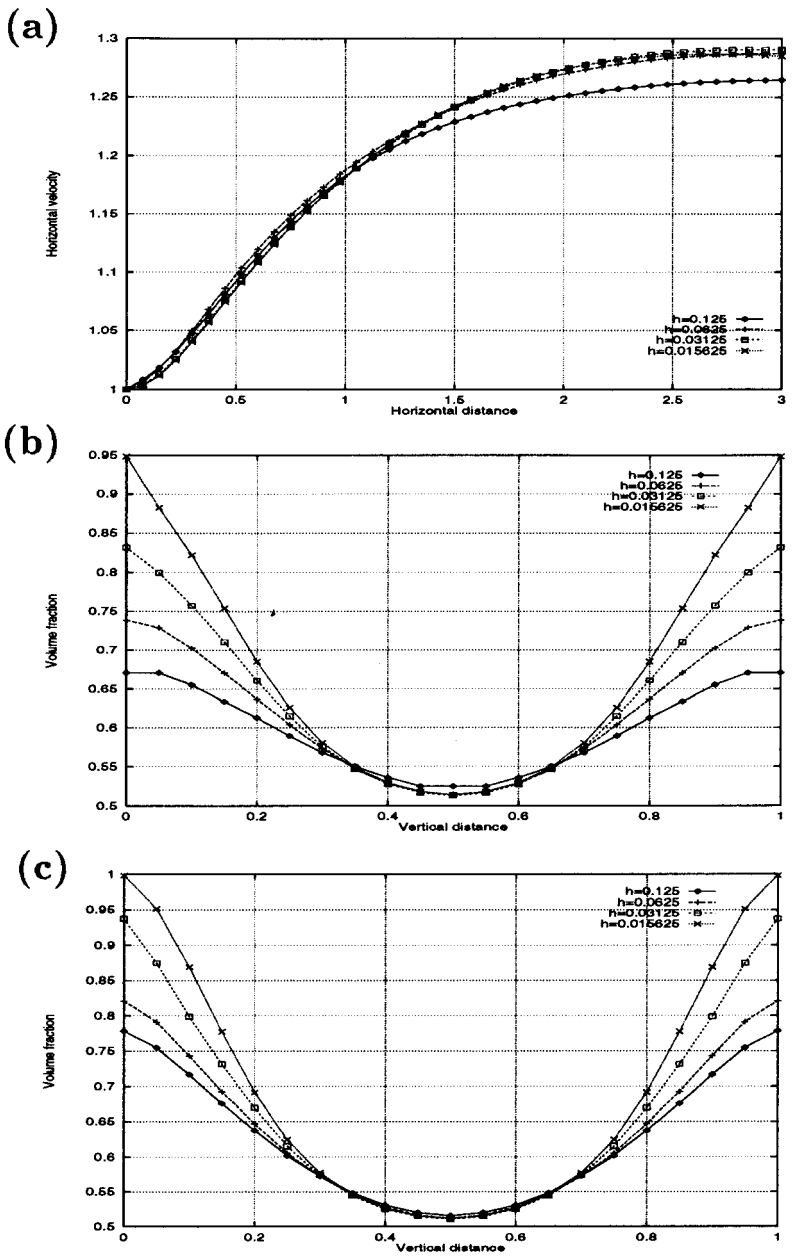

Figure 5. Two-phase channel flow. Grid independence for pamg-multiphase results. (a) Horizontal velocity profiles along the line $y = 0.5$ (phase 1); (b) volume fraction profiles along the line $x = 2.5$ (phase 1); (c) volume fraction profiles along the line $x = 2.5$ (phase 1).

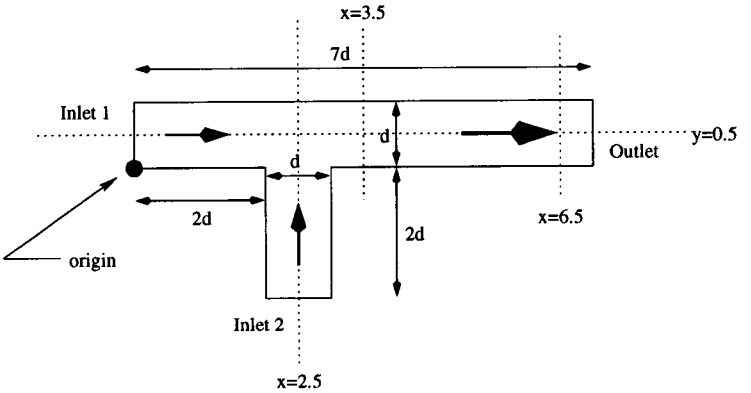

Figure 6. Geometry of the two-phase T-junction problem.

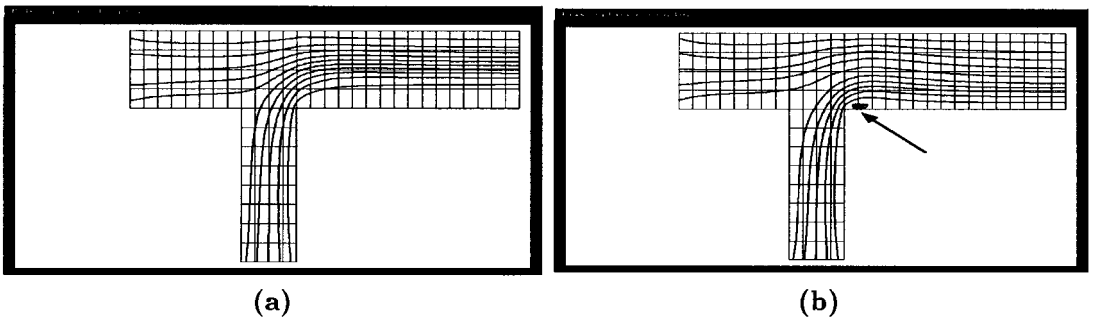

Figure 7. Multiphase T-junction problem. Streamlines for phase 1 (a) and 2 (b). Note the recirculation zone for phase 2.

Note that the inter-phase momentum transfer terms have a stabilising effect on the computations, since they tend to equilibrate the phase velocities. Finally, the coarsest grid (level 1) contains 146 cells and its resolution is $\Delta x_1 = \Delta y_1 = 0.25$.

5.2.2. Flow solution and discussion. Figure 7 shows the streamlines observed for each phase. Some solution profiles are shown in Figure 8. When the junction is reached, the phase with less inertia is forced by the other phase toward the bottom of the exit section of the junction and the flow becomes stratified, as Figure 8(b) clearly shows. Note that gravity is not included in the model.

When the solutions are compared with those provided by CFX 4.1, a very good measure of agreement is again observed. In particular, the pressure drop is correctly estimated (Figure 8(a)). The pamg-multiphase solutions obtained for different grid sizes ($h = \Delta x = \Delta y = 0.0625$ and $h = \Delta x = \Delta y = 0.03125$) have been compared and in sharp contrast to the solutions obtained for the two-phase channel flow, they are significantly more grid-independent (Figure 9).

6. EFFICIENCY OF THE SOLVER

Having validated our implementation, we now turn our attention to the question of the efficiency of the solution algorithm, both in terms of robustness and speed of convergence and computational complexity.

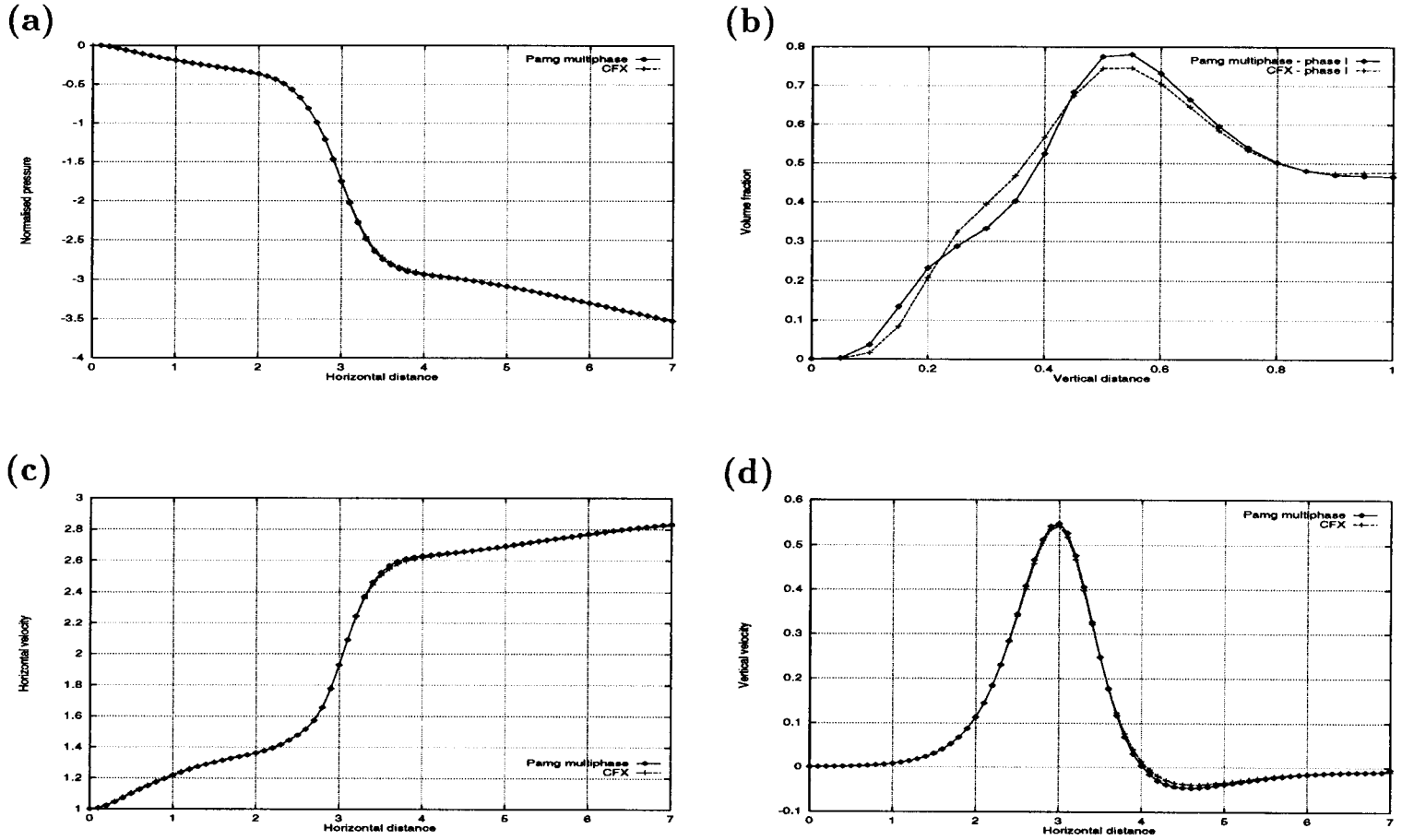

Figure 8. Multiphase T-junction problem. Comparison of pamg-multiphase and CFX 4.1 results. (a): Pressure profiles along the line $y = 0.5$ after normalisation; (b) volume fraction profiles along the line $x = 3.5$; (c) horizontal velocity profiles along the line $y = 0.5$; (d) vertical velocity profile along the line $y = 0.5$.

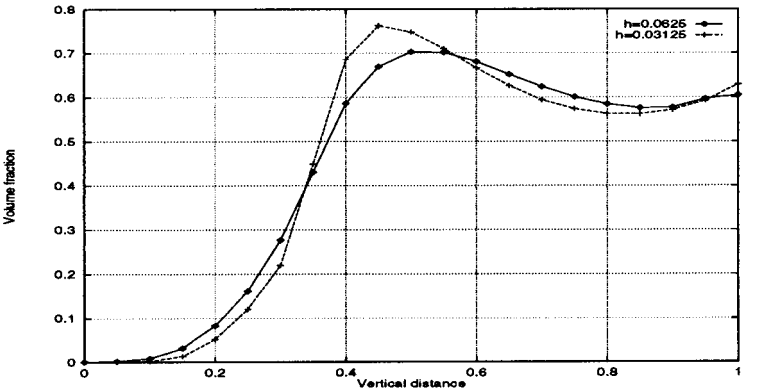

Figure 9. Multiphase T-junction problem. Grid independence for pamg-multiphase results. Volume fraction profiles along the line $x = 6.5$ (phase 1).

6.1. Robustness

The efficiency of the multigrid solver can be assessed using two criteria: the speed of convergence on the one hand, and the robustness of the computations. Because the solution of the problem is obtained on different grids, with different amount of numerical diffusion being added, and since computations always start on the coarsest grid, our solution method implicitly defines a continuation method and is consequently very robust. The convergence of the solver is quite independent from the quality of the initial guess. All results reported here were obtained using unrefined initial guesses: $u = v = p = 0$ and $r_1 = r_2 = 1/2$ on the entire computational domain (except at boundaries).

6.2. Multigrid acceleration

We now turn our attention to the convergence rates and first remark that the FAS multigrid method significantly accelerates the speed of convergence of the single grid quasi-Newton coupled solver. For the two-phase channel flow problem, a three-grid computation using an 'F' cycle is five times faster than the corresponding single grid computation (Figure 10(a)). For the multiphase T-junction problem, the multigrid method works even better as an acceleration technique because it allows a 20-fold increase in speed compared with single grid computations (Figure 10(b)). The comparison here was also carried out on level three uniform grids. The work unit is defined as the cost of one relaxation sweep on the finest grid.

6.3. Muitigrid convergence factors and grid resolution

If a multigrid method works well, one of its benefits is that convergence rates are very largely grid-independent, at least for linear problems. A good multigrid method is therefore an optimal solver (order-wise) for discrete equations. This property was *not* observed for our multiphase computations.

This is particularly striking for the two-phase channel flow problem. Convergence histories for computations where the finest mesh size is $h = \Delta x = \Delta y$ is 1/16, 1/32 and 1/64 respectively, are shown in Figure 11(a). It is obvious that the convergence factors do not scale very well with the mesh size (see Table I).

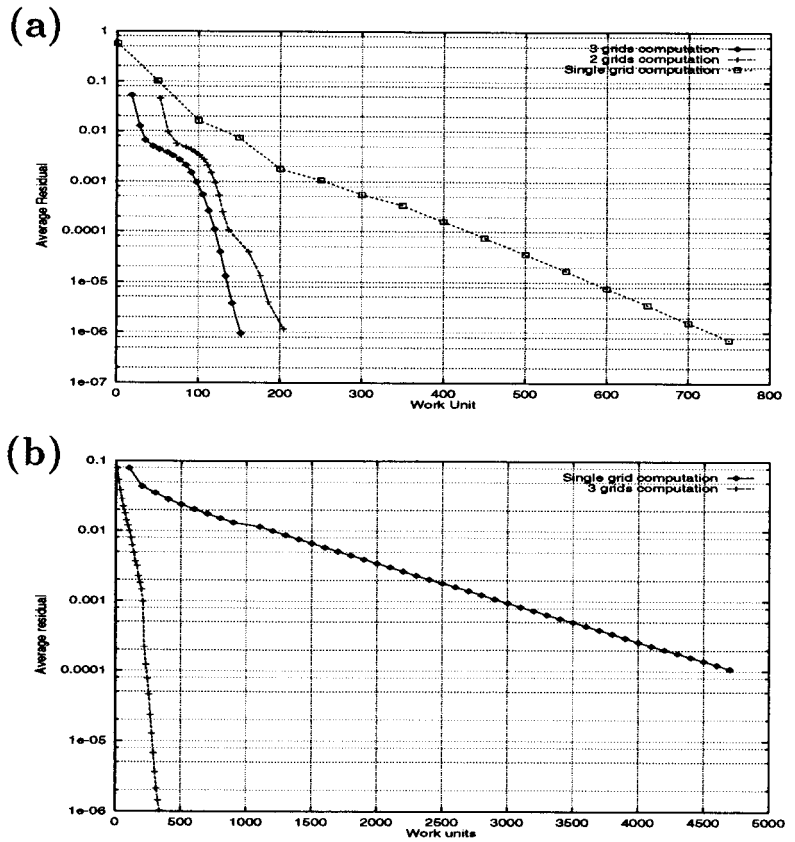

Figure 10. Convergence of solution for multi-grid computations and the equivalent single grid computation. (a) Two-phase channel flow; (b) Two-phase T-junction.

Although FAS is directly applicable to non-linear problems and actually removes the need for a linearisation, a non-linear problem will still be harder to solve because the grid operators, as well as the solutions, must be approximated. For complex non-linear problems the operators may be very different on different grids, and their adjustment (via the defects) will require time. Hence, the dependency of convergence factors on the grid size may primarily be a feature of the multifluid equations. The situation is quite similar to the multigrid simulation of hyperbolic equations: multigrid is a very successful acceleration technique but it is not optimal order-wise [24,25].

Table I. Average convergence factors for the two-phase channel flow problem

Mesh size $h = \Delta x = \Delta y$	Number of cells	Average convergence factor (per relaxation work unit)
0.125	192	0.900
0.0625	768	0.914
0.03125	3 072	0.942
0.015625	12 288	0.964

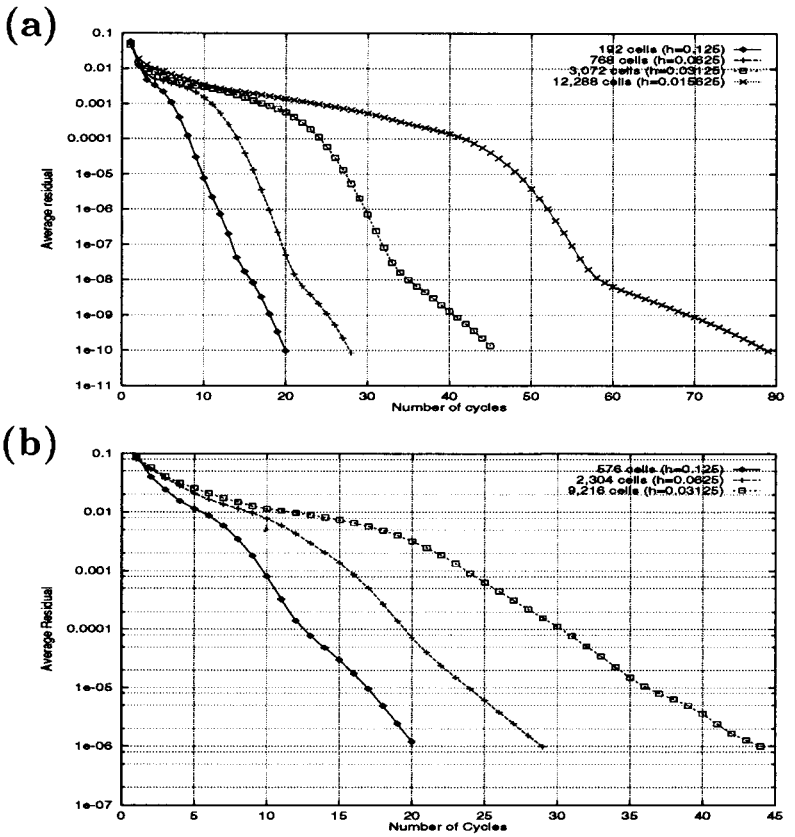

Figure 11. Convergence factors for multigrid computations for different mesh sizes $h = \Delta x = \Delta y$. (a) Two-phase channel flow problem; (b) two-phase T-junction flow problem.

Certainly, grid-independence studies provide support to this argument. They have indicated that multiphase solutions, particularly the volume fraction fields, may be quite sensitive to the grid size. It is interesting therefore to note that for the two-phase T-junction problem, where the volume fractions are more grid-independent, the convergence factors on different grids do not vary so much, as Figure 11(b) and Table II show. It is quite surprising to see that the convergence factor is slightly improved on finer grids although the number of cycles required to obtain convergence is larger. This is due to the fact that the coarse grid (iterative) solver has less and less weight in the multigrid cycle.

Careful examination of Figure 11(a) reveals that in some regions of the convergence history, the convergence factors for the channel problem are almost grid-independent (see Table III). Globally, the history can be divided into three main regions, according to the average residual:

- Up to 10^{-6}, the convergence factors are very grid-dependent. It can be argued that during this phase, the non-linearities are being treated and the approximation of the operators are progressively more accurate. We refer to this as the 'plateau' phase because convergence factors are strongly degraded.

Table II. Average convergence factors for the two-phase T-junction problem

Mesh size $h = \Delta x = \Delta y$	Number of cells	Average convergence factor (per relaxation work unit)
0.125	576	0.9879
0.0625	2304	0.9666
0.03125	9216	0.9656

- Between 10^{-6} and 10^{-8}, convergence factors are grid-independent to a large extent.
- Below 10^{-8}, convergence factors are again grid-dependent. Some evidence (see, e.g. Section 6.4) suggests that this is not a consequence of round-off errors. Rather, it is likely that in this region, another part of the operator dominates.

The properties of the differential operator of interest here are not yet fully understood but a large body of evidence indicates that (non-linear) diffusive effects play a key role in determining the convergence rates of our solver.

6.4. Effect of different formulations of the stress tensor flux

More specifically, the multiphase cross-derivative terms introduced in the diffusive flux $\nabla \cdot (r\mathbf{T})$ are dominant in the 'plateau' phase. These 'extra' diffusive terms further couple the momentum equations together and are analogous to hyperbolic operators. It can be shown that they are associated with spatial variations of the volume fraction.

When the multiphase diffusive terms are omitted, i.e.

$$\nabla \cdot (r\mathbf{T}) = \mu \begin{bmatrix} 2\dfrac{\partial}{\partial x}\left(r\dfrac{\partial u}{\partial x}\right) + \dfrac{\partial}{\partial y}\left(r\dfrac{\partial v}{\partial x}\right) + \dfrac{\partial}{\partial y}\left(r\dfrac{\partial u}{\partial y}\right) \\ \dfrac{\partial}{\partial x}\left(r\dfrac{\partial v}{\partial x}\right) + \dfrac{\partial}{\partial x}\left(r\dfrac{\partial u}{\partial y}\right) + 2\dfrac{\partial}{\partial y}\left(r\dfrac{\partial v}{\partial y}\right) \end{bmatrix}, \tag{24}$$

is replaced by

Table III. Average convergence factors for the two-phase channel flow, depending on the value of the average residual

Mesh size $h = \Delta x = \Delta y$	Average convergence factor			
	to 10^{-4}	between 10^{-4} and 10^{-6}	between 10^{-6} and 10^{-8}	below 10^{-8}
0.125	0.902	0.902	0.906	0.890
0.0625	0.941	0.864	0.876	0.918
0.03125	0.965	0.901	0.886	0.945
0.015625	0.978	0.936	0.896	0.968

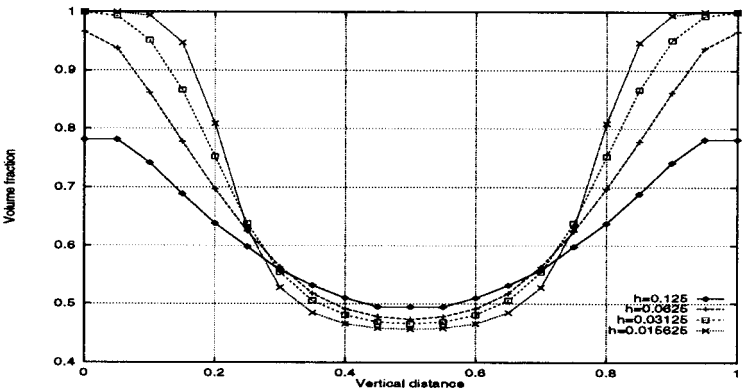

Figure 12. Two-phase channel flow—comparison of volume fraction profiles along the line $x = 2.5$ for the partial diffusion model for different mesh sizes $h = \Delta x = \Delta y$—phase 1.

$$\nabla \cdot (r\mathbf{T}) = \mu \begin{bmatrix} \dfrac{\partial}{\partial x}\left(r\dfrac{\partial u}{\partial x}\right) + \dfrac{\partial}{\partial y}\left(r\dfrac{\partial u}{\partial y}\right) \\ \dfrac{\partial}{\partial x}\left(r\dfrac{\partial v}{\partial x}\right) + \dfrac{\partial}{\partial y}\left(r\dfrac{\partial v}{\partial y}\right) \end{bmatrix}, \tag{25}$$

both the flow solutions and the convergence rates are modified. It clearly appears that the extra terms have a diffusive effect on the volume fraction (compare Figures 5(b) and 12). Because they diffuse the volume fractions, the cross derivative terms actually stabilise the computations.

The slow multigrid convergence factors during the 'plateau' phase can be attributed to the presence of extra terms in the stress tensor flux (compare Figures 13 and 11(a)). We also observe that on fine grids, the degradation of the convergence factors for very low residuals is removed when the extra diffusive terms are turned off. As a result, asymptotic convergence factors are also much more grid-independent (see Table IV) except for grid 5 where, due to the volume fractions tends toward zero and one in certain regions, the conditioning of the quasi-Newton solvers is very significantly worse than on level 4 (see Table V).

Table IV. Multiphase channel flow problem—comparison of global and asymptotic convergence factors for computations on different finest levels for equations with full and partial stress tensor flux $\nabla \cdot (r\mathbf{T})$

Mesh size $h = \Delta x = \Delta y$	Partial diffusion		Full diffusion	
	Global	Asymptotic	Global	Asymptotic
0.125	0.9107	0.9018	0.9004	0.8987
0.0625	0.9230	0.9145	0.9141	0.9031
0.03125	0.9358	0.9115	0.9417	0.9232
0.015625	0.9517	0.9322	0.9636	0.9520

Table V. Comparison of *average* and *maximum* condition numbers of the Newton correction systems on different grid levels, and for computations on different finest levels, with the partial stress tensor flux $\nabla \cdot (r\mathbf{T})$

Grid level	$h = 0.015625$		$h = 03125$	
	Average	Maximum	Average	Maximum
1	7.0×10^1	7.2×10^1	7.1×10^1	7.3×10^1
2	1.7×10^2	2.5×10^2	1.5×10^2	1.6×10^2
3	6.3×10^2	3.5×10^3	3.0×10^2	3.7×10^2
4	5.8×10^3	1.3×10^5	6.1×10^2	1.7×10^3
5	8.4×10^4	5.1×10^6	–	–

7. CONCLUSIONS AND FURTHER WORK

We have applied the FAS multigrid method to the equations governing steady two-dimensional, incompressible viscous two-phase flows in the multifluid model. The (steady) multifluid equations present a level of complexity far higher than their single fluid equivalents: in particular, they are very strongly non-linear, even at small Reynolds numbers.

Our main result is that a symmetrical coupled Gauss–Seidel procedure based on a local quasi-Newton solver which couples locally the discretised equations is of sufficient quality to allow very significant multigrid acceleration, typically by an order of magnitude.

We have also observed that upwind interpolation of the volume fractions in the continuity equations is necessary to obtain a stable discretisation. This is connected with the issue of numerical coupling and second-order-accurate discretisation may be possible. Furthermore, due to the degree of non-linearity of the operator, the Newton step requires the addition of line searching so that it becomes globally convergent.

Associated benefits to our solution strategy are on the one hand, a good degree of robustness since convergence is not dependent on the quality of the initial guess and on the other hand, a natural framework for the implementation of space adaptation. The implementation of adaptive gridding, which can be done in a fully automatic way, will be very beneficial because fine grid resolution is needed in specific regions to accurately resolve the volume fractions. This will be the subject of a further paper.

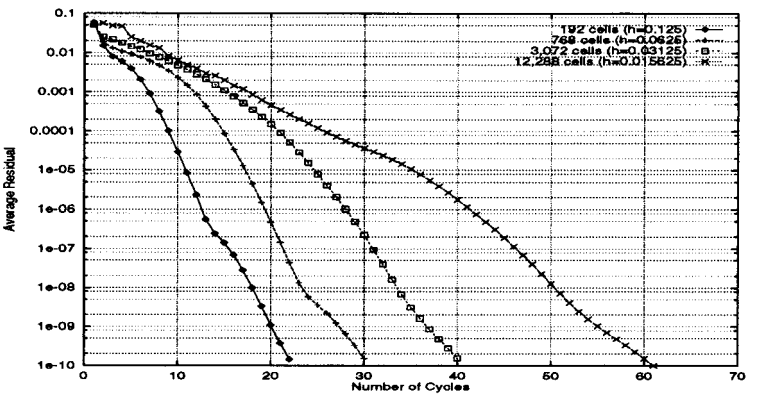

Figure 13. Two-phase channel flow—comparison of the convergence histories for the partial diffusion model for different mesh sizes $h = \Delta x = \Delta y$.

In many cases, the observed convergence rates are not grid-independent. We have highlighted two important factors:

- The operators are very non-linear. Therefore, the adjustment of both the operators and the solutions on different grids (via the FAS defects) will require considerable effort. It has been shown that the volume fraction field can be very grid-dependent.
- Our chosen constitutive relationship for the diffusive stresses involves cross derivative terms which are not well handled by the multigrid method.

Further analysis of the method and the use of techniques such as operator-dependent interpolation [21], may eliminate some of these bottle-necks. This work is in hand. It should be noted that we have been extremely demanding, requiring a reduction of up to nine orders of magnitude in residuals. We have been able to obtain these results in very few cycles. The performance remains very good at more relaxed tolerances.

REFERENCES

1. S.P. Vanka, 'Block implicit multigrid solution of Navier–Stokes equations in primitive variables', *J. Comput. Phys.*, **65**, 138–158 (1986).
2. M.C. Thompson and J.H. Ferziger, 'An adaptive multigrid technique for the incompressible Navier–Stokes equations', *J. Comput. Phys.*, **82**, 94–121 (1989).
3. C.P. Thompson, 'A parallel adaptive multi-grid algorithm for the incompressible Navier–Stokes equations', in *Asymptotic and Numerical Methods for Partial Differential Equations with Critical Parameters (Proceedings of the NATO Advanced Workshop on Asymptotic-Induced Numerical Methods for Partial Differential Equations)*, Kluwer, Dordrecht 1993, pp. 293–309.
4. C.P. Thompson, G.K. Leaf and S.P. Vanka, 'The application of a multi-grid method to a buoyancy-induced flow problem', in S.F. McCormick (ed.), *Multi-grid Methods*, Dekker, New York, 1988, pp. 605–629.
5. C.P. Thompson, W.R. Cowell and G.K. Leaf, 'On the parallelization of an adaptive multigrid algorithm for a class of flow problems', *Parallel Comput.*, **18**, 449–466 (1992).
6. H. Bruce Stewart and B. Wendroff, 'Two-phase flow: models and methods', *J. Comput. Phys.*, **56**, 363–409 (1984).
7. W. Wulff, 'Computational methods for multiphase flow', in G.F. Hewitt, J.M. Delhaye and N. Zuber (eds), *Multiphase Science and Technology*, Vol. 5, Chap. 3, Hemisphere, Washington DC, 1990.
8. A.D. Fitt, 'The numerical and analytical solution of ill-posed systems of conservation laws', *Appl. Math. Model.*, **13**, 618–631 (1989).
9. D.A. Drew, 'Mathematical modelling of two-phase flow', *Annu. Rev. Fluid Mech.*, **15**, 261–291 (1983).
10. G.B. Wallis, *One-Dimensional Two-Phase Flow*, McGraw-Hill, New York, 1969.
11. M. Ishii, *Thermo-Fluid Dynamic Theory of Two-Phase Flow*, Eyrolles, Paris, 1975.
12. D.B. Spalding, 'A novel finite difference formulation for differential expression involving both first and second derivatives', *Int. J. Numer. Methods Eng.*, **4**, 551–559 (1972).
13. P. Lezeau, 'An adaptive quasi-Newton coupled multigrid solver for the simulation of steady multiphase flows', *Ph.D. Thesis*, Cranfield University, 1997.
14. J.D. Pryce and J.K. Reid, 'AD01, a fortran90 code for automatic differentiation', *Technical report*, *Rutherford Appleton Laboratory*, 1996. In preparation.
15. W.H. Press, B.P. Flannery, S.A. Teukolsky and W.T. Vetterling, *Numerical Recipes in C: The Art of Scientific Programming*, 2nd edn, Cambridge University Press, Cambridge, 1992.
16. A. Brandt, 'Multigrid techniques: 1984 guide—with applications to fluid dynamics', in *Computational Fluid Dynamics*, Lecture Series 1984-04, Von Karman Institute, Belgium, 1984.
17. A. Brandt and N. Dinar, 'Multigrid solutions to elliptic flow problems', in S.V. Parter (ed.), *Numerical Methods for Partial Differential Equations*, Academic Press, New York, 1979, pp. 53–147.
18. W.L. Briggs, *A Multigrid Tutorial*, Society for Industrial and Applied Mathematics, 1987.
19. J.H. Bramble, *Multigrid Methods*, Longman, Harlow, 1993.
20. W. Hackbush (ed.), *Multigrid Methods*, Lecture Notes in Mathematics, Vol. 960, Springer, Berlin, 1982.
21. P. Wesseling, *Introduction to Multigrid Methods*, Wiley, New York, 1992.
22. *CFX 4.1 Flow Solver User Guide*, Computational Fluid Dynamic Services, Harwell Laboratory, UK, October 1995.
23. D.B. Spalding, 'Numerical computation of multiphase fluid flow and heat transfer', in C. Taylor and K. Morgan (eds) *Recent Advances in Numerical Methods in Fluids*, Chap. 5, Pineridge Press, Swansea, 1980.
24. W.A. Mulder, 'Multigrid relaxation for the Euler equations', *J. Comput. Phys.*, **60**, 235–252 (1985).
25. W.A. Mulder, 'Analysis of a multigrid method for the Euler equations of gas dynamics in two dimensions', in S. McCormick (ed.), *Multigrid Methods: Theory, Applications and Super-Computing*, Dekker, New York, 1988.

